Springer

KSME

Journal of Mechanical Science and Technology 26 (5) (2012) 1523~1530
www.springerlink.com/content/1738-494x
DOI 10.1007/s12206-012-0337-3

Hydrodynamic study involving a maxblend impeller with yield stress fluids †

Houari Ameur*, Mohamed Bouzit and Mustapha Helmaoui

Faculté de Génie Mécanique, USTO-MB, 1505 El M'nouar, Oran, Algérie

(Manuscript Received August 11, 2011; Revised January 1, 2012; Accepted January 20, 2012)

Abstract

In the present study, the hydrodynamic characteristics of the Maxblend impeller have been investigated. A commercial CFD package (CFX 12.0) was used to solve the 3D hydrodynamics and to characterize the flow patterns at every point. A shear thinning fluid with yield stress was modeled in the laminar regime and transition regime. The study focused on the effect of fluid rheology, agitator speed, impeller clearance from the tank bottom and blade size on the fluid flow and power consumption. Predictions have been compared with literature data and a satisfactory agreement has been found.

Keywords: Hydrodynamic; Maxblend impeller; Power consumption; Stirred vessel; Yield stress fluid

1. Introduction

Mechanically agitated vessels are widely used for various operations within a wide range of industries including the chemical, pharmaceutical, food and petroleum industries. They are used for liquid blending, solid–liquid mixing, gas dispersion in liquids, heat/mass transfer enhancement and chemical reaction.

The general practice for the evaluation of stirred vessels has been done over the years through the experimental investigation for a number of different impellers, vessel geometries, and fluid rheology. Such an approach is usually costly and sometimes is not an easy task. With computational fluid dynamics (CFD), we can examine various parameters contributing to the process with less time and expense, a task otherwise difficult in experimental techniques. During the last two decades, CFD has become an important tool for understanding the flow phenomena [1], developing new processes, and optimizing existing processes [2]. The capability of CFD tools to forecast the mixing behavior in terms of mixing time, power consumption, flow pattern and velocity profiles is considered as a successful achievement of these methods and acceptable results have been obtained. A review of the state-of-the-art in CFD simulations of stirred vessels can be found in Ref. [3].

There is a wide range of mixing geometries available for viscous Newtonian and non-Newtonian fluids, and the selection of an appropriate design for a given application is not an easy task. Several criteria may be used depending on the process requirements, such as specific power consumption, mixing time, pumping efficiency, shear rate distribution and flow field characteristics. The absence of dead zones is of foremost importance for good homogenization.

A new impeller design called Maxblend, the geometry of which is shown in Fig. 1, is one of the most promising new generation wide impellers coming from Japan due to its good mixing performance, lower dissipation and simple geometry, which makes it easy to clean. The Maxblend impeller combines in a single system a paddle surmounted by a grid. The paddle was designed to generate the flow circulation and the grid to provide capacity for dispersing a second liquid, a gas or a solid.

According to the manufacturer [4], the impeller's main advantages are a precise control of the mixing flow in the vessel and the generation of a relatively uniform shear contrary to open turbines, where high shears are located in the vicinity of the turbine.

However, detailed information regarding the Maxblend performance is limited. Kouda et al. [5] and Hiruta et al. [6] have employed Maxblend in fermentation processes in aerated conditions showing very competitive mass transfer coefficients while keeping the broth culture very well mixed. Sumi and Kamiwano [7] have investigated some mixing characteristics of Maxblend with highly viscous fluids and compared it with multistage impellers. A numerical investigation on dispersive mixing of the Maxblend and a comparison with helical ribbons impellers has also been carried out [8]. They concluded that in deep laminar regime, the Maxblend cannot reach an effective dispersive mixing. The Maxblend power consump-

*Corresponding author. Tel.: +213 770343722
E-mail address: houari_ameur@yahoo.fr
† Recommended by Associate Editor Byeong Rog Shin.

tion and solid suspension performance in gas–liquid–solid applications were also investigated and compared with other large-scale impellers [9]. They found out that the Maxblend creates a more uniform solid suspension in comparison to Fullzone and triple impellers. The mixing performance of Maxblend and other large impellers in boiling stirred tank reactors was investigated by Takahashi et al. [10], who found that the Maxblend has essentially the same performance as the other impellers in this application. Numerical and experimental comparisons of Maxblend with double helical ribbon (DHR) were carried out by Takahashi et al. [11]. They concluded that although Maxblend and DHR have almost the same power consumption, Maxblend has longer mixing time where $Re<10$ and shorter where $Re>10$.

However, Maxblend cannot generate enough circulation in deep laminar regime. These characteristics of the Maxblend have been later confirmed by Iranshahi et al. [12] in an experimental and numerical study.

Both Fradette et al. [13] and Devals et al. [14] have been interested in the mixing of Newtonian and power law fluids. Patel et al. [15] have studied with experiments the power consumption for mixing pseudoplastic fluid possessing yield stress. Rivera et al. [16] has modeled the laminar and transition flow of the Superblend dual shaft coaxial mixer using Newtonian fluid.

A thorough search of the literature suggests that no space has been devoted to the numerical simulation of the agitation of yield stress fluid with Maxblend impellers. Therefore, the objective of the present paper is to employ advanced computational fluid dynamics (CFD) to study the flow patterns and power consumption for stirring shear thinning fluids possessing yield stress with this type of impeller. Our attention is focused on the effect of the Reynolds number, fluid rheology, impeller clearance from the tank bottom, and the blade size.

2. Description of the stirred system

The Maxblend impeller considered in this work is shown in Fig. 1. All the geometrical parameters for both of the vessel and impeller are given in Table 1.

The objective of the present work was to investigate several design parameters affecting the performance of this type of agitator. The effect of impeller clearance from the tank bottom was analyzed. At this end, four geometrical configurations were realized which are: c/D = 0.016, 0.1, 0.18 and 0.26, respectively. Also, the influence of blade size has been tested (d/D = 0.535, 0.625, 0.750 and 0.937).

3. Numerical issues

The commercially available computer code (CFX 12.0) developed by AEA Technology, UK, was used to simulate the steady state 3D flow field generated by a Maxblend impeller. CFX is a general purpose computer program using a finite volume method. The Navier-Stokes equations written in a rotating, cylindrical frame of references are solved. Because of the choice of a rotating frame, two terms are added to the equations: centrifugal and Coriolis accelerations. The equations are written in terms of velocity components and pressure. These variables are discretized on a grid of control volumes, which enables a more precise mass conservation, and a faster convergence. A pressure-correction method of the type Semi-Implicit Method for Pressure- Linked Equations-Consistent (SIMPLEC) is used to perform pressure-velocity coupling.

Table 1. Tank and impeller characteristics in mm.

d	*di*	*h1*	*h2*	*D*	*Ds*	*H*
225	110	75	170	300	10	360

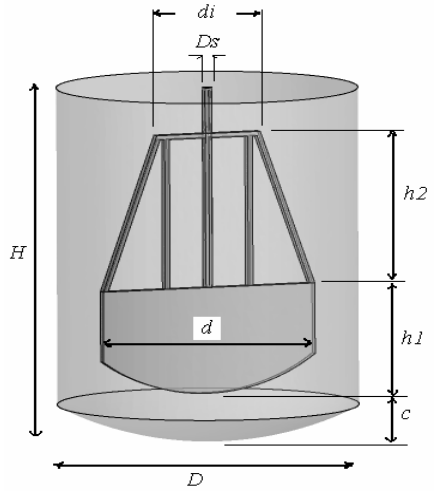

Fig. 1. Stirred system.

Constant boundary conditions have been set respecting a rotating reference frame (RRF) approach. Here, the impeller is kept stationary and the flow is steady relative to the rotating frame, while the outer wall of the vessel is given an angular velocity equal and opposite to the velocity of the rotating frame. This approach can be employed due to the absence of baffles. The same RRF approach, often used for stirred vessels, has given accurate results for several different stirring systems [17, 18]. The simplification of the stirring system where baffles have been removed is obviously independent of the CFD resolution and is only due to mixing and industrial considerations. In the case of agitated vessels involving baffles, computational flow could nonetheless have been easily achieved with an MRF [18] or sliding meshes approaches.

A pre-processor (ICEM CFD 12.0) was used to discretize the flow domain with a tetrahedral mesh (Fig. 2). An increased mesh density was used near the impeller and the tank walls in order to capture the boundary layer flow details. Mesh tests were performed by verifying that additional cells did not change the velocity magnitude in the regions of high velocity gradients around the impeller blades by more than 2.5%.

To verify the grid independency, the number of cells was increased by a factor of about 2 used by other researchers in

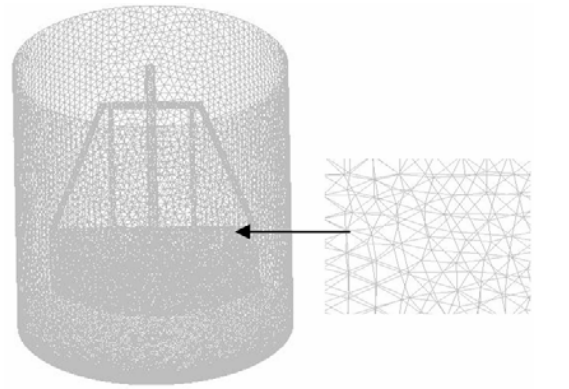

Fig. 2. Numerical grid (tetrahedral mesh).

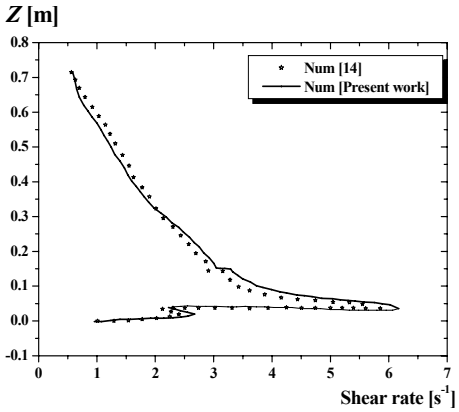

Fig. 3. Shear rate for $Re = 4$, $n = 0.9$.

CFD modeling of the mixing processes [19, 20]. The original 3D mesh of the model had 121,252 computational cells. To verify the grid independency, the number of cells was increased from 121,252 cells to 242,504 cells. The additional cells changed the velocity magnitude in the regions of high velocity gradients and the impeller power number by more than 3%. Thus, the number of cells was changed from 242,504 cells to 485,008 cells. The additional cells did not change the velocity magnitude in the regions of high velocity gradients and impeller power number by more than 2.5%. Therefore, 242,504 cells were employed in this study.

Simulations were considered converging when the scaled residuals for each transport equation were below 10^{-7}. The velocities had converged to either a single value. Most simulations required about 1000 iterations for convergence. Computations were carried out using Pentium(R) Dual Core CPU 2.20 GHz with 2.0 GB of RAM and convergence was typically achieved after 4 – 6 h.

4. Theoretical background

Shear thinning fluids with yield stress were modeled in this work, the Xanthan gum solution was considered. It's rehology can be described by the Herchel Bulkkley model [21]:

$$\tau = \tau_y + K\dot{\gamma}^n \tag{1}$$

where τ_y is the yield stress, K is the consistency index, $\dot{\gamma}$ is the shear rate and n is the flow behavior index.

According to the Metzner and Otto's correlation [22], the average shear rate can be related to the impeller speed by:

$$\dot{\gamma}_{avg} = K_s N \tag{2}$$

where K_s is a weak function of impeller type. The average shear rate can be used to evaluate the apparent viscosity (η) of the solution, which is a Herschel-Bulkley fluid (Eq. (1)).

$$\eta = \frac{\tau}{\dot{\gamma}_{avg}} = \frac{\tau}{K_s N} = \frac{\tau_y + K\left(K_s N\right)^n}{K_s N} \tag{3}$$

The Reynolds number can be given as:

$$Re_y = \frac{K_s N^2 D^2 \rho}{\tau_y + K\left(K_s N\right)^n}. \tag{4}$$

Table 1 summarizes the rheological properties of the different Xanthan gum solutions used in this work, which are based on measurements conducted by Galindo and Nienow [23].

The power consumption is a macroscopic result obtained by integration on the impeller surface of the local power transmitted by the impeller to the fluid. It is quite equivalent to say that the power consumption P is entirely given by the impeller to the fluid. In these conditions:

$$P = \eta \int_{vessel\ volume} Q\, dv. \tag{5}$$

The element dv is written as:

$$dv = r\, dr\, d\theta\, dz \tag{6}$$

$$Q_v = \left(2\tau_{rr}^2 + 2\tau_{\theta\theta}^2 + 2\tau_{zz}^2 + \tau_{rz}^2 + \tau_{r\theta}^2 + \tau_{z\theta}^2\right)/\eta^2 \tag{7}$$

$$\tau_{rr} = -\eta\, 2\partial v_r/\partial r \tag{8}$$

$$\tau_{r\theta} = -\eta\left[r\partial\left(v_\theta/r\right)/\partial r + \left(1/r\right)\partial v_r/\partial\theta\right] \tag{9}$$

$$\tau_{rz} = -\eta\left[\partial v_r/\partial z + \partial v_z/\partial r\right]. \tag{10}$$

The power number is calculated according to this equation:

$$N_P = \frac{P}{\rho N^3 D^5}. \tag{11}$$

5. Results and discussion

To validate the CFD model, similar geometrical conditions to those chosen by Devals et al. [14] were considered. For shear thinning fluid modeled by the Oswald law, the predicted results for shear rate as a function of the vessel height are shown in Fig. 3 and compared with those given by Devals et

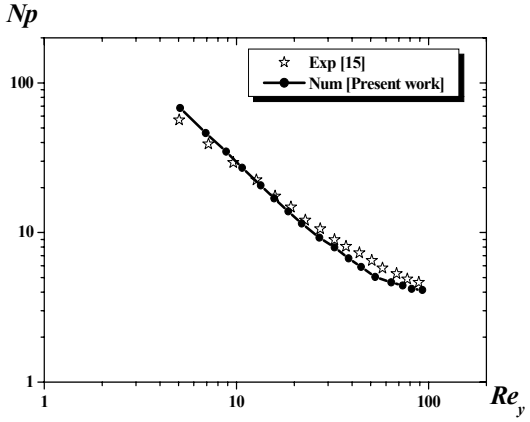

Fig. 4. Power number (Np) versus Reynolds number (Re_y) (1.5% xanthan gum).

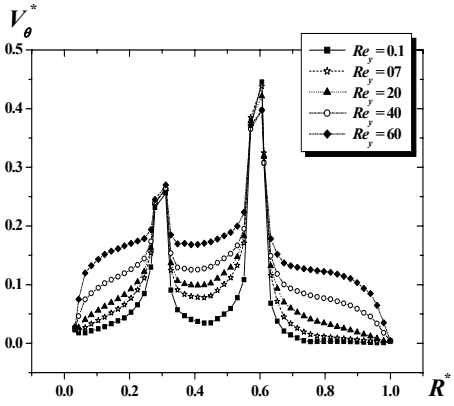

Fig. 5. Tangential velocity for n = 0.18, c/D = 0.016, d/D = 0.75, Z^* = 0.55, $\theta = 0^0$.

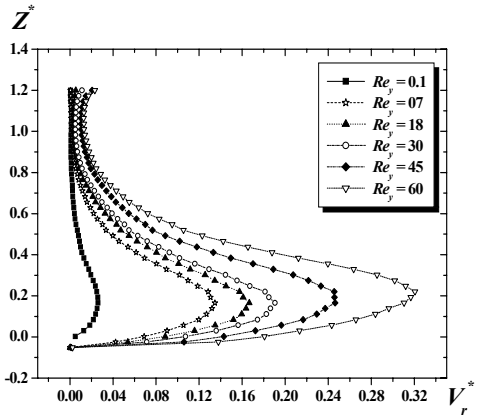

Fig. 6. Radial velocity for n = 0.18, c/D = 0.016, d/D = 0.75, R^* = 0.6, $\theta = 90^0$.

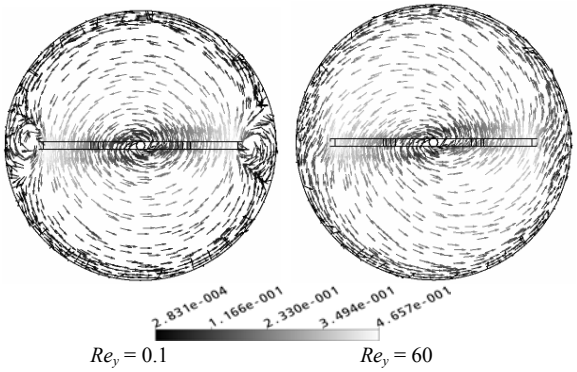

Fig. 7. Comparison of the segregated zone for n = 0.18, c/D = 0.016, d/D = 0.75, Z^* = 0.16.

al. [14].

Another validation is made (Fig. 4) which concerns a comparison of predicted power number with measured data given by Patel et al. [15]. The fluid used here is shear thinning with yield stress. As illustrated, the comparison shows a satisfactory agreement.

5.1 Effect of Reynolds number

We begin the analysis by testing the effects the impeller rotational speed on the flow fields generated. The origin of tangential coordinate (θ) is located on a paddle. Fig. 5 shows the variations of tangential velocity along the blade and its extension at the grid region of the impeller. It can be clearly seen that the velocity increases rapidly to reach up its maximum at the blade tip, and begins to fade when moving away from the mechanical source, until becomes neglected on the tank wall. On the other hand, the decay curve is faster when the Reynolds number is weak.

Following the variations of radial velocity along the vessel height (Fig. 6), we remark that this variable is important in the area swept by the paddle part of the agitator. The magnitude of this variable increases with respect to Re_y.

The agitation of yield stress fluids result in the formation of zone of intense motion near the impeller (the so called cavern) with essentially stagnant and/or slow moving fluids elsewhere [24, 25].

At a low Reynolds number, Re_y = 0.1, the circulation of fluid particles is low intense (Fig. 7), but the increase of Re_y (Re_y = 60) yields higher shear rates. The sufficient impeller rotational speed can eliminate the vortex generated at the each side of the impeller blade and increases the axial circulation of fluid and cavern size.

Fig. 8 shows the flow velocity field in a vertical cross section plane (the plane orthogonal to the impeller) at four different Reynolds numbers, namely 5, 30, 65 and 120.

The paddle at the vessel bottom produces a strong tangential flow and a weak axial flow, generating a strong recirculation at the vessel bottom that causes flow segregation. Above the paddle, the grid part generates an axial pumping, with an upward motion at the vessel wall and a downward flow along the shaft.

For this impeller location and because of the great clearance from the tank bottom (c/D = 0.26), the flow will be divided into two streams when the Reynolds number increases (Re_y =

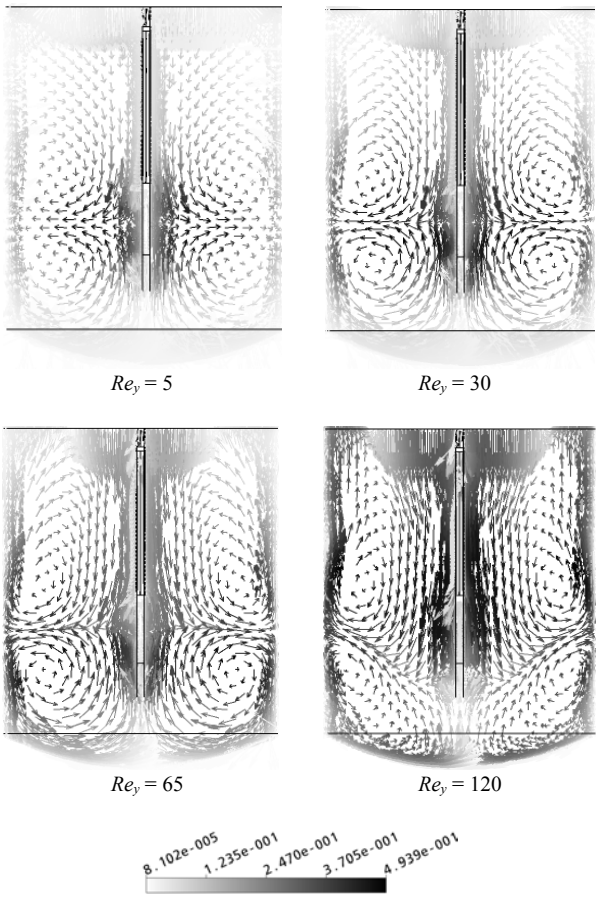

Fig. 8. Velocity vectors for n = 0.18, c/D = 0.26, d/D = 0.75.

30 and 65), one downward to the vessel bottom and other to the free surface of liquid, forming then tow recirculation loops. But the continued increase of Re_y enhances the axial pumping and the velocity field seems more intense with a better exchange with the main circulation loop (Re_y = 120).

On Fig. 9, we can remark that in the bottom region, the fluid stretching is more intense at higher values of the Reynolds number. At the top of the vessel, the value of the shear rate is pretty low, which corresponds to a quasi-solid body rotation. Clearly, the distance between the upper part of the impeller and the liquid surface in the vessel must be adjusted if one wants to ensure mixing in this region.

5.2 Effect of fluid rheology

The fluid rheology has also an important effect on the flow fields generated. Two cases are chosen to perform the test (Table 2).

The profiles of tangential velocity component plotted on Fig. 10 show that the velocity maximum is located in the area swept by the impeller. This variable decreases slowly to become negligible at the tank wall. The continuous increase in structural index yields higher shear rate in the vicinity of the impeller because of the viscous forces, which generate larger

Table 2. Rheological properties of Xanthan gum solutions.

Concentration (%)	K [Pa s^n]	n [-]	τ_y [Pa]
1.5	14.5	0.12	7.1
3.5	33.1	0.18	20.6

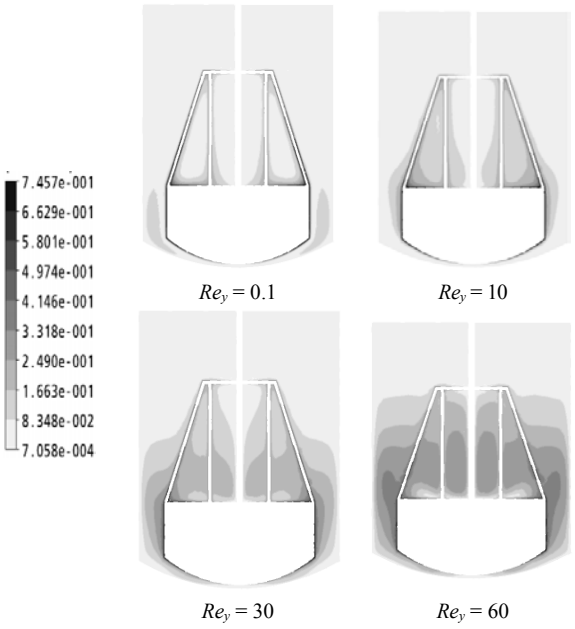

Fig. 9. Velocity contours for n = 0.18, c/D = 0.016, d/D = 0.75.

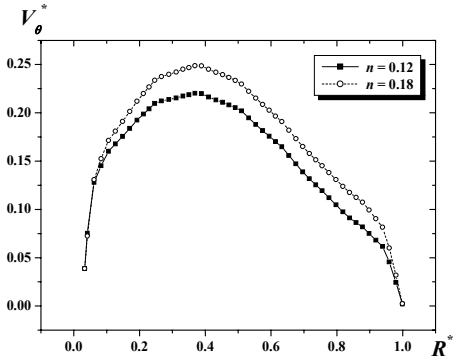

Fig. 10. Tangential velocity for Re_y = 60, c/D = 0.016, d/D = 0.75, Z^* = 0.5, $\theta = 90^0$.

well-stirred region. The contours presented on Fig. 11 illustrate this phenomenon more clearly.

The power consumption constitutes a global parameter to describe the performances of a mechanically stirred system. Fig. 12 presents the variations of Np versus of Re_y in a logarithmic scale, and it can be seen that at Reynolds number less than 10 the line with the slope of −1 fits the data quite well. In the transition regime, the power number changes slightly with Re_g. On the other hand, the power number is presented for different values of power law index. It is clear that Np increases in respect with n, and this is due to the viscous forces.

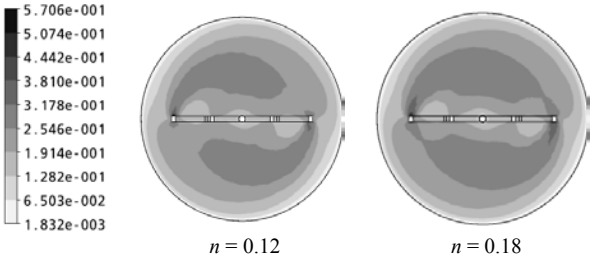

Fig. 11. Velocity contours for $c/D = 0.016$, $d/D = 0.75$, $Z^* = 0.36$, $Re_y = 60$.

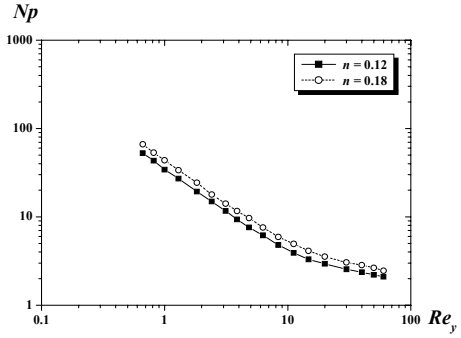

Fig. 12. Power number for $c/D = 0.016$, $d/D = 0.75$.

5.3 Effect of impeller clearance

The effect of the bottom clearance has been investigated in this section, as, according to the manufacturer, the magnitude of the clearance can have a noteworthy influence on the mixing efficiency. In the study, the dimensionless clearance ratio c/D was varied from 0.016 to 0.26.

Fig. 13 shows the flow velocity field in two vertical cross section planes (the Maxblend plane) at two different impeller clearances, namely 0.016, 0.26. The normal velocity vector to the plane has been removed from the pictures to highlight the secondary flow. The top-to bottom pumping induced by the Maxblend is remarkable: the flow goes upward near the wall and downward in the center along the shaft. In Fig. 14 and for the first case ($c/D = 0.016$) a small recirculation zone can be noticed in the wake of the bottom paddle in agreement with the experimental observation of Fradette et al. [14].

At the same figure (Fig. 14), is shown a comparison of the velocity field for $Re_y = 60$ in the vertical cross-section for two different clearance values: 0.016 and 0.26. From the details of the bottom vortex in Fig. 14, a close analysis of the velocity field shows that the flow patterns are sensitive to the bottom gap size, only one circulation loop is marked for the very little clearance ($c/D = 0.016$). With the larger clearance, the bottom recirculation size has increased (two recirculation loops are formed) and the velocity field seems more intense with a better exchange with the main circulation loop.

Fig. 15 highlights more clearly the size of vortices generated for different ratios of c/D. the sign minus indicates the existing of recirculation loops.

Fig. 16 shows the evolution of the power number Np versus

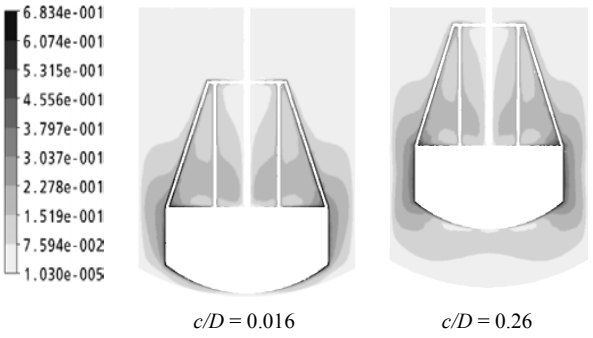

Fig. 13. Velocity contours for $Re_y = 60$, $n = 0.18$, $d/D = 0.75$, $\theta = 0^0$.

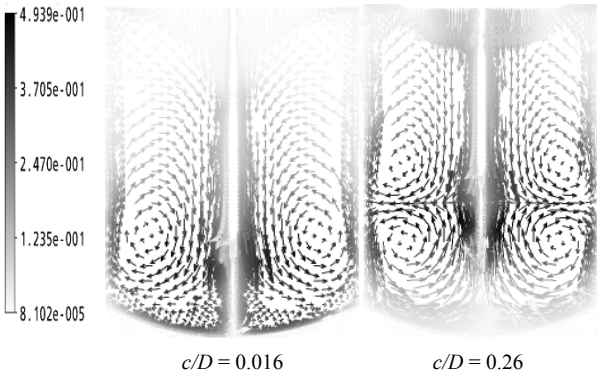

Fig. 14. Velocity vectors for $Re_y = 60$, $n = 0.18$, $d/D = 0.75$, $\theta = 90^0$.

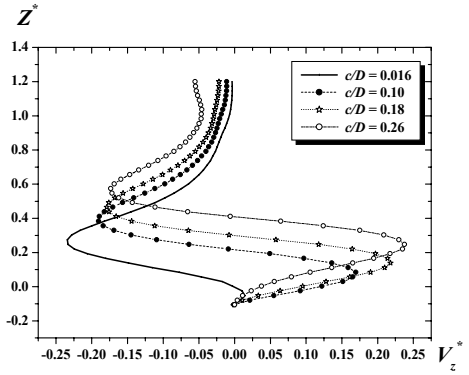

Fig. 15. Axial velocity for $Re_y = 60$, $n = 0.18$, $\theta = 90^0$, $R^* = 0.16$, $d/D = 0.75$.

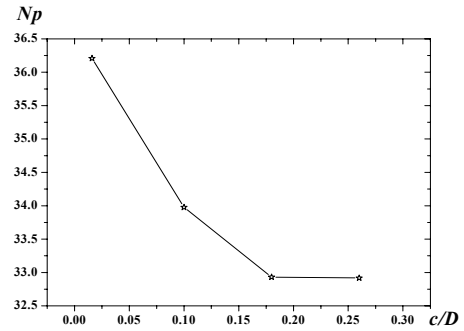

Fig. 16. Power number for $Re_y = 1.5$, $n = 0.18$, $d/D = 0.75$.

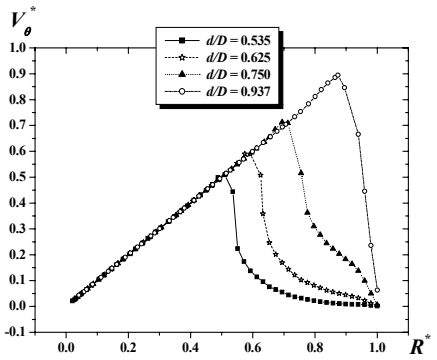

Fig. 17. Tangential velocity for Re_y = 60, n = 0.18, Z^* = 0.2, c/D = 0.1.

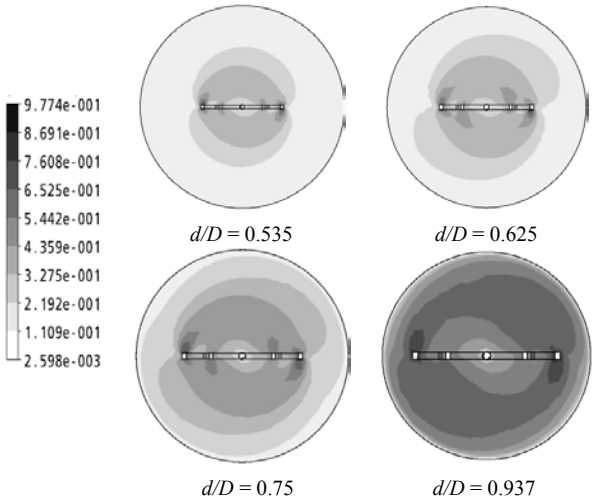

Fig. 18. Velocity contours for Re_y = 60, n = 0.18, Z^* = 0.66, c/D = 0.1.

c/D. It can be seen that the power number varies non-linearly with the clearance value. A significant increase in power is obtained when the clearance is decreased with respect to its nominal value. On the other hand, the drop in power is moderate when the gap is increased.

5.4 Effect of the blade size

The effect of blade width on the flow patterns and power consumption has also been studied. To perform this test, four geometrical configurations have been realized, which are: d/D = 0.535, 0.625, 0.75 and 0.937 respectively.

The variations of tangential velocity component along the vessel radius and for the four cases studied are plotted on Fig. 17. At the paddle part of the agitator and along its extension, we remark that the velocity maximal is located at the blade tip for any of the cases investigated, but the pic is more pronounced with respect to d/D.

The area swept by the impeller becomes greater with the increase in blade width, the cavern size is then larger (Fig. 18), but the required power consumption is more significant when compared at the same Reynolds number and same structural index (Table 3).

Table 3. Power number for Re_y = 16, n = 0.18, c/D = 0.1.

d/D	0.535	0.625	0.750	0.937
Np	3.13	4.66	7.65	13.93

6. Conclusion

A CFD characterization of the hydrodynamics of the Maxblend impeller has been carried out in the laminar and transition regime with yield stress fluids.

The upper corner of impeller grid is a critical area. Poor mixing is observed in this region when the Reynolds number and impeller clearance are weak, so it is better to modify this part of impeller.

The bottom clearance value also plays an important role: not only is less power needed as the gap size increases, but better exchange between the bottom recirculation and the main circulation loop is obtained with a larger clearance. The segregated zones diminish by increasing the Reynolds number.

The increase in blade size is beneficial to enlarge the cavern volume, but that requires more power consumption.

Nomenclature

c : Impeller off-bottomed clearance (m)
d : Paddle diameter (m)
di : Diameter of the impeller grid (m)
$h1$: Paddle height (m)
$h2$: Grid height (m)
n : Power law index (dimensionless)
D : Tank diameter (m)
Ds : Diameter shaft (m)
H : Vessel height (m)
K : Consistency index (Pa s^n)
K_s : Metzner-Otto's constant (dimensionless)
N : Impeller rotational speed (1/s)
P : Power (W)
Np : Power number (dimensionless)
Q_v : Viscous dissipation function ($1/s^2$)
Re_y : Yield stress Reynolds number (dimensionless)
V : Velocity (m/s)
V_z : Axial velocity (m/s)
V_θ : Tangential velocity (m/s)
V_r : Radial velocity (m/s)
γ : Shear rate (1/s)
$\dot{\gamma}_{avg}$: Average shear rate (1/s)
τ : Shear stress (Pa)
τ_y : Suspension yield stress (Pa)
ρ : Fluid density (kg/m^3)
η : Apparent viscosity (Pa s)

References

[1] P. M. Armenante, C. Luo, C. C. Chou, I. Fort and J. Medek, Velocity profiles in a closed, unbaffled vessel: comparison

between experimental LDV data and numerical CFD prediction, *Chem. Eng. Sci.* 52 (20) (1997) 3483-3492.

[2] A. K. Sahu, P. Kummar and J. B. Joshi, Simulation of flow in stirred vessels with axial flow impellers: zonal modeling and optimization of parameter, *Ind. Eng. Chem. Res.* 37 (6) (1998) 2116-2130.

[3] M. Sommerfeld and S. Decker, State of the art and future trends in CFD simulation of stirred vessel hydrodynamics, *Chem. Eng. Tech.* 27 (3) (2004) 215-224.

[4] Sumitomo Heavy Industries, available at http://www.shi.co.jp/maxblendclub/e-index.html.

[5] T. Kouda, H. Yano and F. Yoshinaga, Effect of agitator configuration on bacterial cellulose productivity in aerated and agitated culture, *J. Ferm. Bioeng.* 83 (2) (1997) 371-376.

[6] O. Hiruta, K. Yamamura, H. Takebe, T. Futamura, K. Iinuma and H. Tanaka, Application of Maxblend fermentor for microbial processes, *J. Ferm. Bioeng.* 83 (1) (1997) 79-86.

[7] Y. Sumi and M. Kamiwano, Development and mixing characteristic of multistage impeller for agitating highly viscous fluid, *Chem. Eng. Jpn.* 34 (4) (2001) 485-492.

[8] W. Yao, M. Mishima and K. Takahashi, Numerical investigation on dispersive mixing characteristics of Maxblend and double helical ribbons, *Chem. Eng. J.* 84 (3) (2001) 565-571.

[9] N. Dohi, T. Takahashi, K. Minekawa and Y. Kawase, Power consumption and solid suspension performance of large-scale impellers in gas–liquid–solid three-phase stirred tank reactors, *Chem. Eng. J.* 97 (3) (2004) 103-114.

[10] K. Takahashi, H. Horiguchi, M. Mishima and R. Yatomi, Mixing characteristics in a vessel agitated by large paddle impeller Maxblend, *Proc. of 12th European Conference on Mixing,* Bologna*,* Italy (2006).

[11] T. Takahashi, A. Tagawa, N. Atsumi, N. Dohi and Y. Kawase, Liquid phase mixing time in boiling stirred tank reactors with large cross-section impellers, *Chem. Eng. Proc.* 45 (4) (2006) 303-311.

[12] A. Iranshahi, C. Devals, M. Heniche, L. Fradette, P. A. Tanguy and K. Takenaka, Hydrodynamics characterization of the Maxblend impeller, *Chem. Eng. Sci.* 62 (4) (2007) 3641-3653.

[13] L. Fradette, G. Thome, P. A. Tanguy and K. Takenaka, Power and mixing time study involving a Maxblend impeller with viscous Newtonian and non Newtonian fluids, *Chem. Eng. Res. Des.* 85 (11) (2007) 1514-1523.

[14] C. Devals, M. Heniche, K. Takenaka and P. A. Tanguy, CFD analysis of several design parameters affecting the performance of the Maxblend impeller, *Comp. Chem. Eng.* 32 (8) (2008) 1831-1841.

[15] D. Patel, F. Ein-Mozaffari and M. Mehrvar, Improving the dynamic performance of continuous-flow mixing of pseudo-plastic fluids possessing yield stress using Maxblend impeller, *Chem. Eng. Res. Des.* 90 (4) (2011) 514-523.

[16] C. A. Rivera, M. Heniche, K. laminar and transition flow of *Chem. Eng. Sci*. 64 (21) (2009) 4442-4456.

[17] J. Aubin, I. Naude, C. Xuereb and J. Bertrand, Blending of Newtonian and shear-thinning fluids in a tank stirred with a helical screw agitator, *Trans. Inst. Chem. Eng.* 78 (4) (2000) 1105-1114.

[18] I. Naude, Direct simulations of impellers in a stirred tank: Contribution to the optimization of the choice of an agitator, *Ph.D. thesis,* INPT, France (1998).

[19] B. Letellier, C. Xuereb, P. Swaels, P. Hobbes and J. Bertrand, Scale-up in laminar and transient regimes of a multi-stage stirrer, a CFD approach, *Chem. Eng. Sci.* 57 (21) (2002) 4617-4632.

[20] V. Buwa, A. Dewan, A. F. Nasser and F. Durst, Fluid dynamics and mixing of single-phase flow in a stirred vessel with a grid disc impeller: experimental and numerical investigations, *Chem. Eng. Sci*. 61 (9) (2006) 2815-2822.

[21] C. W. Macosko, *Rheology: Principles, measurements & applications*, Wiley-VCH, New York (1994).

[22] B. Metzner and R. E. Otto, Agitation of non-Newtonian fluids, *AIChE J.* 3 (1) (1957) 3-11.

[23] E. Galindo and A. W. Nienow, The performance of the Scaba 6SRGT agitator in the mixing of simulated xanthan gum broths, *Chem. Eng. Technol.* 16 (2) (1993) 102-108.

[24] L. Pakzad, F. Ein-Mozaffari and P. Chan, Using computational fluid dynamics modeling to study the mixing of pseudoplastic fluids with a Scaba 6SRGT impeller, *Chem. Eng. and Proc.* 47 (12) (2007) 2218-2227.

[25] L. W. Adams and M. Barigou, CFD analysis of caverns and pseudo-caverns developed during mixing of non-Newtonians fluids, *Chem. Eng. Res. Des.* 85 (5) (2007) 598-604.

Houari Ameur was born in 1982 in Tlemcen, Algeria. He received his degree of engineer in marine engineering and master in mechanical engineering at the University of Science and Technology, Oran, Algeria. He is a Ph.D student in rheology of complex fluids. His current research interests are mainly in the area of non-Newtonian fluid flows, mechanical mixing and computational fluid dynamics.